RSC Advances

ROYAL SOCIETY OF CHEMISTRY

PAPER

Cite this: *RSC Adv.*, 2025, **15**, 6938

Insights into the fungal secretomes and their roles in the formation and stabilization of the biogenic silver nanoparticles†

Thyerre Santana da Costa, ‡ Gonzalo García Delgado, ‡ Carolyne Brustolin Braga and Ljubica Tasic *

The biosynthesis of silver nanoparticles (AgNPs) using biological systems has emerged as a promising alternative to traditional chemical methods, providing eco-friendly solutions in nanotechnology. This study investigates the secretomes of two strains of *Fusarium oxysporum* (VR039 and 07SD) to synthesize AgNPs (AgNP@Fo VR039 and AgNP@Fo 07SD), characterized by similar sizes of 35.4 ± 12.4 nm and 28.6 ± 9.5 nm, respectively. We conducted proteomic analysis *via* mass spectrometry on both secretomes and nanoparticles, identifying proteins involved in the biosynthesis, stabilization, and antimicrobial activity of the nanoparticles. Our results indicate notable similarities in the proteomes of both nanoparticles and their respective secretomes, correlating with similar antimicrobial efficacy against *Staphylococcus aureus* and *Escherichia coli*, as demonstrated through bacterial growth inhibition assays. The presence of redox proteins, such as glyceraldehyde reductase and FAD-oxidoreductase, suggests a potential mechanism for the generation of reactive oxygen species (ROS) and oxidative stress in bacterial cells, further validated by fluorescence microscopy to differentiate viable from non-viable cells. Unlike previous studies that have focused separately on metal ion reduction or nanoparticle stabilization, our findings reveal a coordinated biosynthetic process where the same proteins mediate both functions. This overlap between the secretome and nanoparticle proteome provides new insights into fungal-mediated nanoparticle synthesis, highlighting the multifunctionality of fungal proteins in bionanotechnology. By demonstrating how secreted enzymes directly contribute to nanoparticle formation, this study paves the way for more efficient, scalable, and environmentally sustainable approaches to biogenic nanoparticle production.

Received 8th November 2024
Accepted 18th February 2025

DOI: 10.1039/d4ra07962k

rsc.li/rsc-advances

1. Introduction

Silver nanoparticles (AgNPs) have emerged as key candidates in a broad spectrum of scientific and technological applications, driving innovations in the biological and medical fields.[1–7] However, the synthesis and stabilization of AgNPs often involve chemical methods that include reducing and stabilizing agents, potentially posing environmental and human health risks.[8,9] At this juncture, the biosynthesis of AgNPs using reducing molecules from microorganisms emerges as an innovative and environmentally sustainable alternative.[10,11] The ability of microorganisms, such as the fungus *Fusarium oxysporum* f. sp. *cubense*, to synthesize and stabilize AgNPs, opens new frontiers for the sustainable production of these highly valuable biomaterials.

Microorganisms, including bacteria and fungi, can convert metal ions into nanoparticles through a series of biochemical reactions. This ability is often attributed to the presence of specific enzymes, peptides, and biomolecules within their cellular machinery.[12,13] These bioactive molecules act as both reducing and stabilizing agents, controlling the size, shape, and properties of the resulting bionanoparticles.[14] The utilization of microbial systems for nanoparticle biosynthesis offers several advantages. Firstly, the process occurs under mild conditions, minimizing energy consumption and reducing the production of hazardous waste. Secondly, the use of microorganisms provides a renewable source of bioactive compounds, which can be tailored through genetic engineering or environmental modifications. Lastly, biogenic nanoparticles tend to exhibit enhanced biocompatibility,[15–17] antibacterial and anticancer activity based on ROS generation, and membrane permeability making them promising candidates for applications such as drug delivery in antibacterial and anticancer therapies among other applications in the nano-biology field.[18,19] However, several limitations must be considered. Fungal filtrate composition can vary depending on the culture medium[20] and fungal strain,[21] which may affect the

Institute of Chemistry, Biological Chemistry Laboratory, Universidade Estadual de Campinas, UNICAMP, Campinas, SP, 13083-970, Brazil. E-mail: ljubica@unicamp.br

† Electronic supplementary information (ESI) available. See DOI: https://doi.org/10.1039/d4ra07962k

‡ These authors contributed equally to this work.

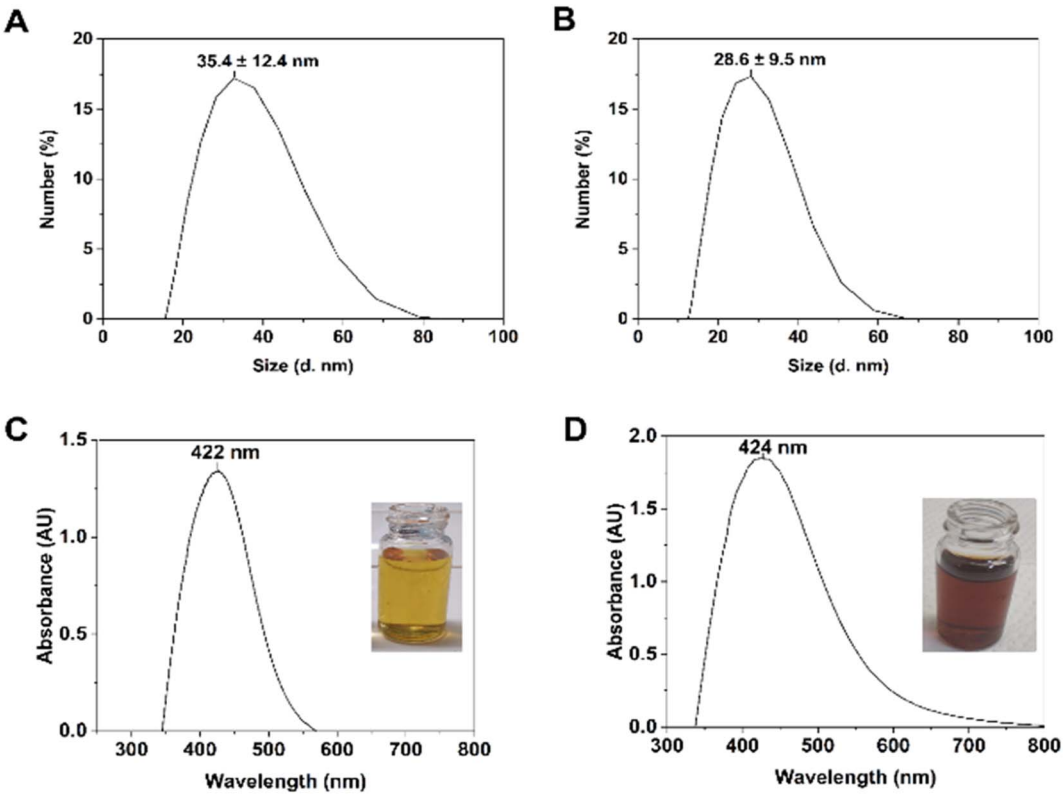

Fig. 1 Characterization of the synthesized silver nanoparticles using *Fusarium oxysporum* f. sp. *cubense* (AgNP@Fo). Characterization techniques: (A) DLS size distribution diagram of AgNP@Fo VR039 showing an average hydrodynamic size of 35.4 ± 12.4 nm, (B) DLS size distribution diagram of AgNP@Fo 07SD showing an average hydrodynamic size of 28.6 ± 9.5 nm, (C) UV-vis absorption spectrum of silver nanoparticles (AgNP@Fo VR039) with a maximum at 422 nm, (D) UV-vis absorption spectrum of AgNP@Fo 07SD with a maximum at 428 nm.

characteristics and properties of the synthesized nanoparticles,[22,23] and make the nanoparticle synthesis optimization challenging. Additionally, the underlying mechanisms of nanoparticle formation remain poorly understood due to the complexity of biomolecules present in the secretome, highlighting the need for further investigation and standardization.

Microorganisms are known to produce molecules and proteins that can be used in the synthesis of biogenic nanoparticles. However, there is still a knowledge gap regarding the molecules involved in this process, particularly concerning the proteins that participate in the biosynthesis and stabilization of the nanomaterial.[24,25] Identifying these macromolecules and understanding their functions not only offer insights into the mode of action of biogenic AgNPs but also hold promise for understanding the cytotoxicity of the nanomaterial and for more personalized and targeted applications in biological systems.[26–29]

In a previous study, our group reported a technique for the biological synthesis of AgNPs using a filtrate from the secretome of the fungus *Fusarium oxysporum* (namely AgNP@Fo).[30] The synthesized spherical AgNP@Fo exhibited antimicrobial activities against a variety of bacteria, including both Gram-positive and -negative strains, and demonstrated anticancer activity against hepatocarcinoma cells (Huh-7). The current experimental work, through proteomic analysis, was designed to investigate and describe the proteins associated with AgNP@Fo and to assess the involvement of these macromolecules in the synthesis process, stability, and their synergistic potential with the silver nanoparticles to enhance the antimicrobial capacity of the nanomaterial.

2. Results and discussion

The size of the nanoparticles was determined through DLS analysis, revealing that AgNP@Fo VR039 had an average hydrodynamic diameter of 35.4 ± 12.4 nm (Fig. 1A), with zeta-potentials of −21.8 ± 6.6 mV, and polydispersity index (PDI) of 0.48. Furthermore, AgNP@Fo 07SD exhibited an average diameter of 28.6 ± 9.5 nm (Fig. 1B), displayed zeta potentials of −27.2 ± 5.9 mV, and polydispersity of 0.42. A PDI between 0.42 and 0.48 suggests a size distribution that is not fully monodisperse but still reasonably controlled. In the case of nanoparticles biosynthesized by fungal secretomes, which involves a biological process that is not entirely controlled, such a PDI range is well-accepted, indicating that the biosynthesis process is yielding a certain degree of uniformity, even without the strict control methods typically used in chemical syntheses.[31] Both types of silver nanoparticles exhibited surface plasmon resonance (SPR) at around 420 nm (Fig. 1C and D), characteristic of spherical silver nanoparticles.[32]

To assess the morphology of the biosynthesized nanoparticles, AgNP@Fo VR039 was used as the test model. TEM

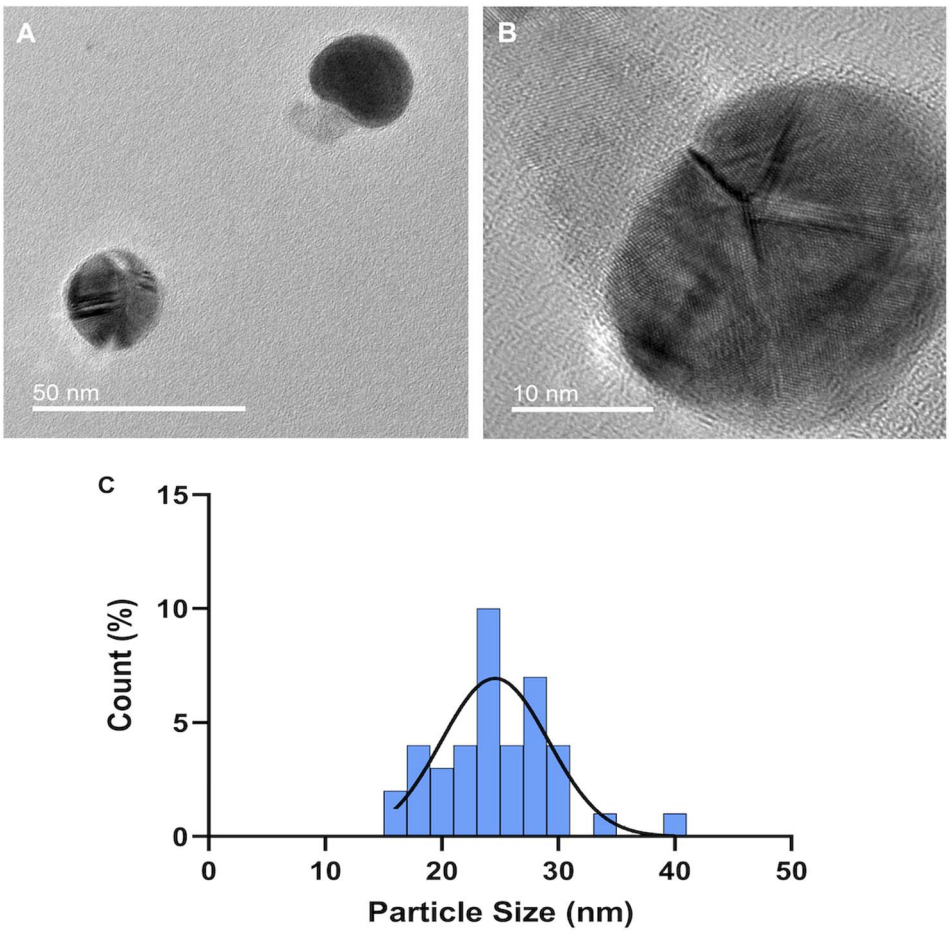

Fig. 2 (A and B) TEM images of silver nanoparticles AgNP@Fo VR039. (C) Size distribution diagram of the nanoparticles, showing the average size 24.5 ± 3.7 nm calculated using ImageJ software.

(Fig. 2) analysis revealed spherical morphology of the nanomaterials, which is typically observed in silver nanoparticles synthesized from fungal secretomes.[33] The average size of AgNP@Fo VR039 measured by TEM was 24.5 ± 3.7 nm, which is close to the size calculated by DLS.

Energy-dispersive X-ray (EDX) elemental analysis was conducted alongside TEM (Fig. 3A–D), providing elemental details of the components near the surface of the silver nanoparticles and their overall positional mapping. Based on the EDX results, carbon was the most abundant element present in the colloids, originating from the fungal extract used in the biosynthesis of AgNP@Fo. Silver and copper were also detected, with smaller amounts of chlorine, sulfur, and silicon.

Fungi, bacteria, and plant extracts are recognized for their ability of providing the precursors for the biosynthesis of silver nanoparticles, utilizing the reducing potential of enzymes (Fig. 4A). The proteins secreted by *Fusarium oxysporum* strains exhibited a wide range of isoelectric points, typically falling between pH 5 and 9. Their molecular masses also showed significant variation, ranging from 11 to 130 kDa. Among the fungal proteins, we identified glucan 1,3-β-glucosidase, β-glucosidase, cuticle-degrading protease, glucoamylase, serine/threonine-protein kinase, glyceraldehyde reductase, FAD-oxidoreductase, and others (ESI†).

All these proteins are involved in the metabolic pathways of the fungi like hydrolases, oxidoreductases, proteases, and transferases, some with functions of defense, and transport (Fig. 4B).

Protein quantification in both the fungal filtrate samples and the AgNP@Fo colloids was performed using the Bradford method with bovine serum albumin (BSA) as the standard protein, Fig. 4C.

Upon analyzing the data, it became evident that the quantity of the proteins in the AgNP samples was approximately 14 times lower than in the fungal filtrates. This suggests that not all the proteins secreted by *F. oxysporum* are likely involved in the synthesis or stabilization of the produced AgNP@Fo.

A Venn diagram revealed a high similarity among the reductase proteins present in the fungal filtrates (Fig. 5B) and the nanoparticles (Fig. 5C), such as FAD-linked oxidoreductase, glyceraldehyde reductase, and glutathione reductase, which could play essential roles in reducing silver ions for nanoparticle formation. Additionally, other proteins with varied functions were identified, including cuticle-degrading protease, aspartyl aminopeptidase, glucoamylase, 10 kDa mitochondrial heat shock protein, chitinase A1, oxygen-dependent

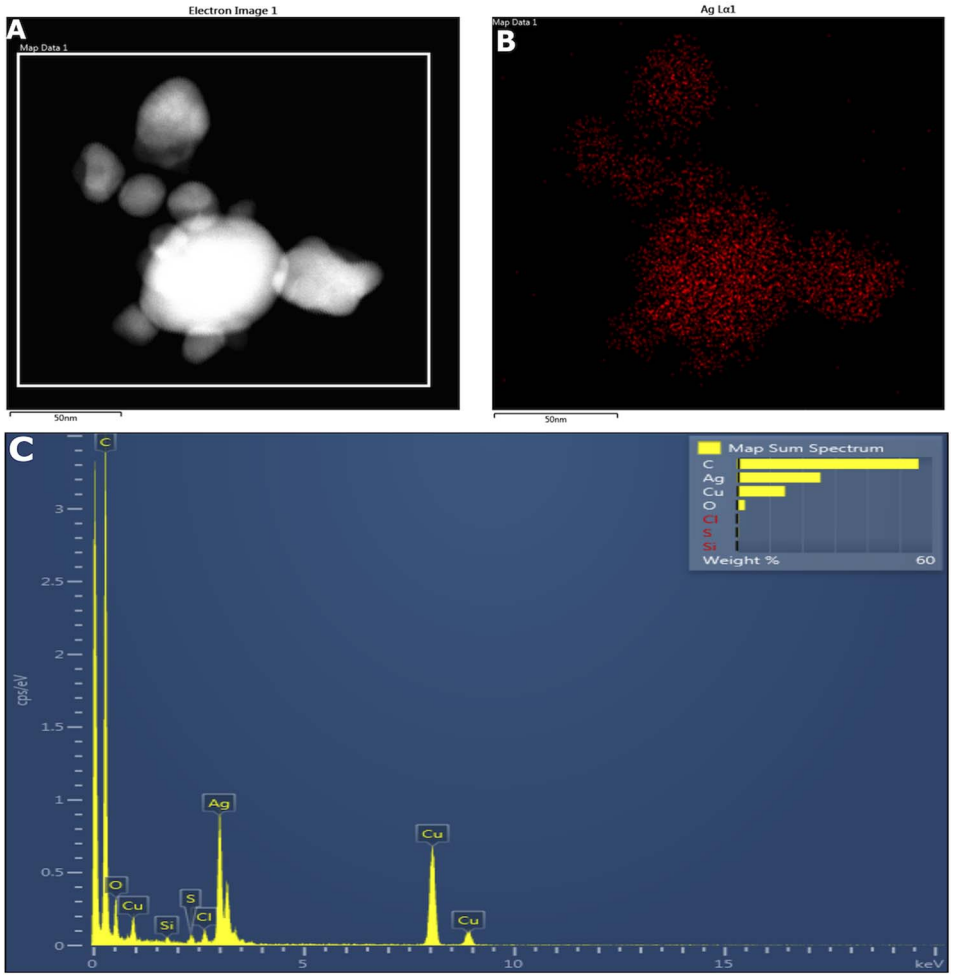

Fig. 3 Analysis of the silver nanoparticles AgNP@Fo VR039. (A) Electron microscopy image of the nanoparticles. (B) Silver contour within the nanoparticles. (C) EDX spectrum and elemental mapping of the electron micrograph region.

coproporphyrinogen-III oxidase, ribose-5-phosphate isomerase, ribonuclease Trv invertase, and xylosidase/arabinosidase. Further details regarding these proteins, including their sequences, coverages, molecular masses, and scores, can be found in the ESI,† and Table 1.

Forty-one (41) proteins were successfully identified in both nanoparticle reaction media, encompassing proteins classified as putative and hypothetical. The detailed protein classification can be found in Fig. 6. A majority of the identified proteins within the nanoparticle media play crucial roles in *F. oxysporum*'s virulence and defense mechanisms. Notably, enzymes such as glucosidases and chitinases are utilized for the degradation of plant cell walls, while ribonucleases and proteases perform defensive purposes. Additionally, oxidoreductases are instrumental in *F. oxysporum*'s defense against reactive oxygen species.

In this study, all hypothetical proteins were categorized using the standard BLAST protein–protein algorithm, specifically by selecting a minimum of four proteins with an identity of 64% or higher. The hypothetical protein Foc1_g10004489 exhibited significant identity with proteins containing a GLEYA domain in their sequences. This domain is associated with proteins found in adhesive fungi, such as *F. oxysporum*, known for colonizing host plants and forming biofilms.[34] The hypothetical proteins Foc1_g10009336 and Foc1_g10003812 show at least 69% and 98% identity with the carbohydrate-binding wall stress component (WSC) membrane protein, respectively, the last one plays an important role in the fungus stress response. The WSC domain has up to eight conserved cysteine residues that can form disulfide bonds[34] and act as a stress sensor, activating a signaling cascade, usually, activating other proteins with hydrolytic activity, bringing oxidation protection to the cell wall or degrading toxic molecules.[35–37] The hypothetical protein Focb16_v008394 shows a high identity with proteins that belong to the alpha/beta hydrolases, a family of proteins that could be peptidases, esterases, lipases, epoxidase among others, proteins that can be related to cellular protection or surface determination.[38,39]

The hypothetical proteins Foctr4_00003641 and Foctr4_00015075 also belong to the hydrolases superfamily, being identified as carboxypeptidase A4 and chitinase I, respectively, with 99% identity. Carboxypeptidases A4 are

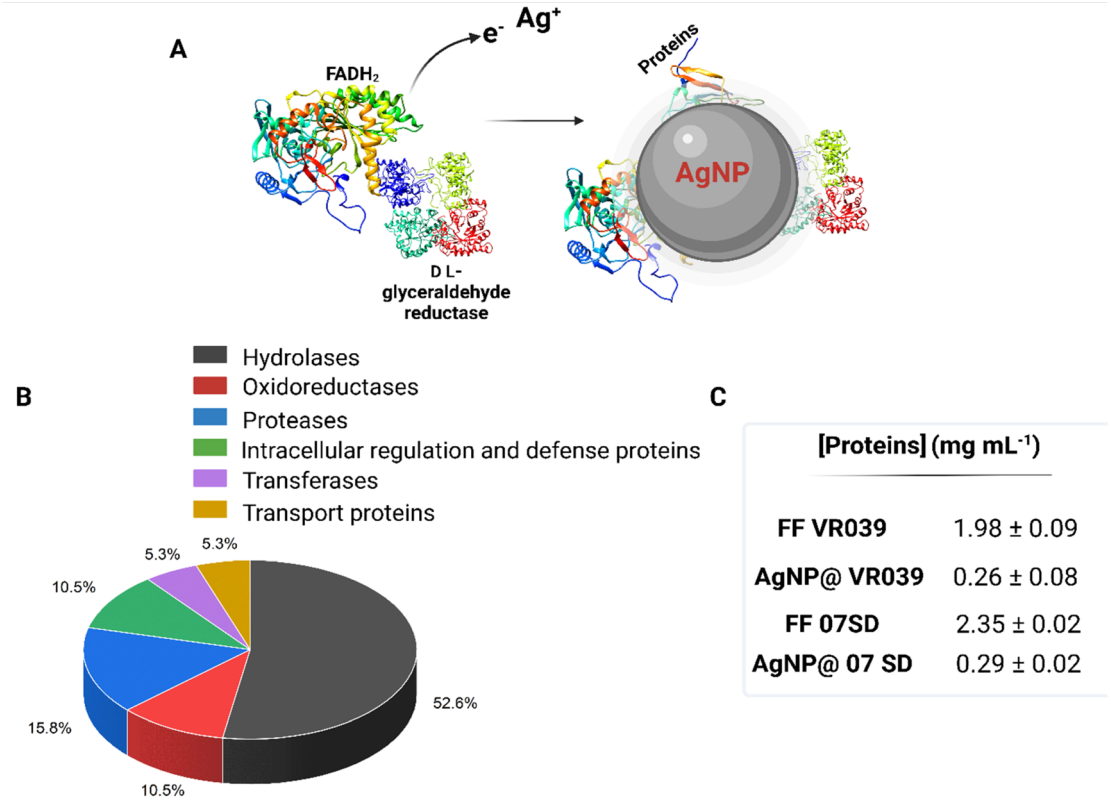

Fig. 4 (A) Biogenic synthesis of silver nanoparticles *via* Ag^+ reduction mediated by redox-active proteins, (B) protein composition ratio identified within silver nanoparticles, (C) protein concentration measured by Bradford assay present in the fungal filtrate (FF) VR039 and the fungal filtrate (FF) 07SD, AgNP@Fo VR039, and AgNP@Fo 07SD.

peptidases that are specialized in C-terminal hydrophobic small residue removal[41] and are usually used by *F. oxysporum* to avoid plant chitinase activity as a result of plant immune response.[42] The plants use chitinases to attack the fungus, hydrolyzing β-1,4-*N*-acetyl-D-glucosamine linkages present in cell wall structure but those proteins are also used by fungi as a defense mechanism against other fungus ou to degrade host cell wall.[43] Chitinases also participate in poly-*N*-acetylglucosamine biosynthesis, degrading the biopolymer to release *N*-acetylglucosamine that is used by the fungus to synthesize the biopolymer again as a part of the cell wall reparation.[44] This can explain the presence of the hypothetical protein Foc1_g10014191, which has a high identity to class I glutamine amidotransferase, a protein that is present in fungi under stress conditions and increases the chitin presence in the cell wall.[45] Finally, three more hypothetical proteins were identified, Foctr4_00016438 that is recognized as a cell wall glycoprotein with a DNA polymerase III subunit γ/τ conserved domain, and protein Foctr4_00002732, identified as 40S ribosomal protein S5, both proteins participate in DNA transcription and translation. The last protein, Foctr4_00009577, was identified as a hydrophobic, cysteine-rich protein that is present in the fungi filament.

Various fungal-derived materials are used in the synthesis of biogenic nanoparticles, including fungal extracts and secretomes, which facilitate the formation of different types of nanoparticles. For example, a study by Mohammadhassan and collaborators described how sulfite oxidoreductase catalyzed the oxidation of NAD(P)H, transferring electrons that reduce Au^{3+} to form metallic gold (Au^0).[46] Similarly, research by S. Xue and colleagues discussed how thiol groups in fungal proteins can reduce selenite to generate selenium nanoparticles.[47] Despite these advances, the precise mechanisms underlying fungi-assisted biogenic nanoparticle synthesis remain unclear.[3]

In a study conducted by our research group, we demonstrated that in a bottom-up approach, nanoparticle formation occurs through the aggregation of smaller units, such as atoms or molecules, leading to nanoparticle assembly. Specifically, in the case of silver nanoparticle (AgNP) synthesis by fungi, redox proteins present in the secretomes played a crucial role in reducing silver ions (Ag^+) to metallic silver (Ag^0), which subsequently formed nanoparticles. Key redox proteins, including glucoamylases, glyceraldehyde reductases, and FAD-oxidoreductases, act as reducing agents by donating electrons to Ag^+ ions, thereby facilitating their reduction to Ag^0. This redox-mediated process is essential for the nucleation and growth of silver nanoparticles. In addition to their role in ion reduction, these proteins also contribute to nanoparticle stabilization by preventing aggregation and forming protective layers composed of proteins or functional groups, ensuring the stability of the nanoparticles for future applications.[24,30] Some proteins and their potential roles are shown in Table 1.

To evaluate the antimicrobial potential of the nanoparticles AgNP@Fo VR039 and AgNP@Fo 07SD, the bacteria

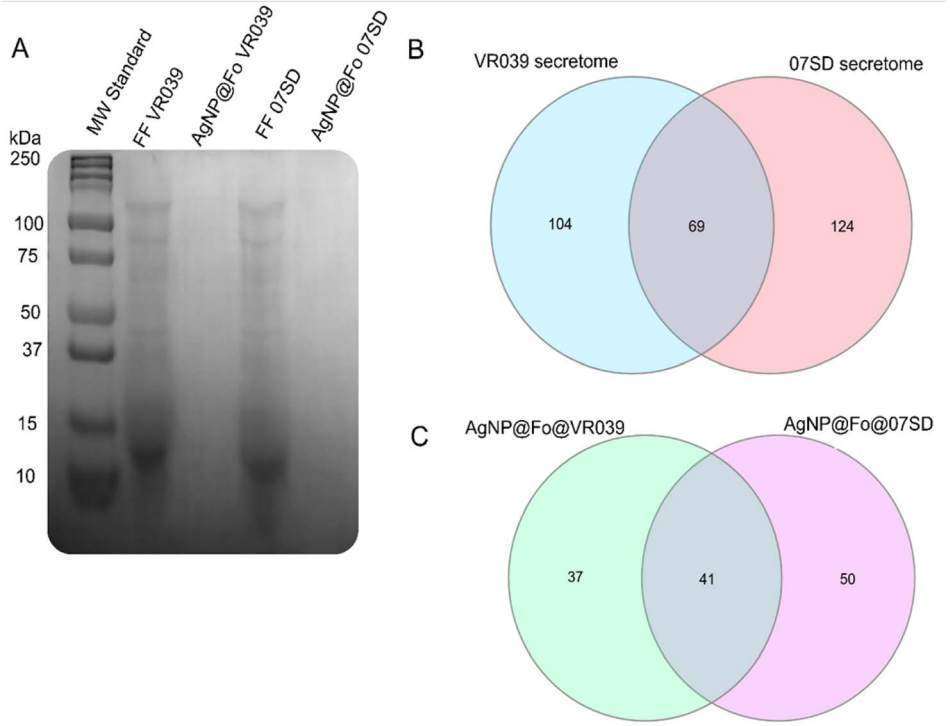

Fig. 5 (A) A 12% SDS-PAGE gel stained with Coomassie blue, first lane corresponds to the molecular marker, second lane corresponds to the *Fusarium oxysoporum* VR039 fungal filtrate, third lane shows the AgNP@FoVR039 proteins, fourth lane shows the *Fusarium oxysoporum* 07SD fungal filtrate and the fifth lane shows the AgNP@Fo 07SD proteins; (B) Venn diagram[40] of the intersection of the proteins identified in the secretome of different *Fusarium oxysporum* strains (VR039 and 07SD); (C) Venn diagram of the intersection of the proteins identified in the nanoparticles AgNP@Fo VR039 and AgNP@Fo 07SD.

Staphylococcus aureus (*S, aureus*, Gram-positive) (Fig. 7A) and *Escherichia coli* (*E. coli*, Gram-negative) (Fig. 7B) were used, maintaining the same concentration of nanoparticles in both tests. Analysis through ANOVA ($p < 0.0001$) revealed that both nanoparticles exhibited similar biological potential against these bacteria, both Gram-positive and Gram-negative. This

Table 1 List of the identified proteins in the synthesized silver nanoparticles (AgNP@Fo VR039 and AgNP@Fo 07SD) and their potential roles

Protein	Potential role
Minor extracellular protease Vpr	Degrades extracellular proteins, generating peptides that may contribute to nanoparticle stabilization
Carboxypeptidase Cpds	Cleaves peptide bonds at protein termini, influencing the availability of stabilizing peptides for nanoparticles
Putative extracellular serine carboxypeptidase	Hydrolyzes peptide bonds, potentially enhancing nanoparticle stabilization through peptide interactions
Putative aspartic-type endopeptidase	Facilitates protein degradation, releasing peptides that may stabilize nanoparticles
β-Glucosidase 4, 5 and 6	Hydrolyzes glycosidic bonds, potentially contributing to nanoparticle stabilization *via* carbohydrate interactions
Glycosyl hydrolase 5 family protein	Modifies complex carbohydrates, releasing smaller carbohydrate molecules that may aid nanoparticle stabilization
Putative glycosidase Crf1 and Crf2	Involved in carbohydrate processing, potentially influencing nanoparticle stability through carbohydrate interactions
Putative leucine aminopeptidase 2 and 3	Participates in proteolysis, generating peptides that may assist in nanoparticle stabilization
Carbohydrate-binding WSC domain-containing protein	Binds to carbohydrates, likely playing a role in nanoparticle capping and surface stabilization
FAD oxidoreductase	Catalyzes redox reactions, potentially facilitating silver ion reduction and nanoparticle synthesis
Glyceraldehyde reductase	Contributes to redox homeostasis, influencing nanoparticle formation by modulating the reduction environment
Putative secreted lipase	Modifies lipid structures, potentially affecting nanoparticle–protein interactions and aggregation

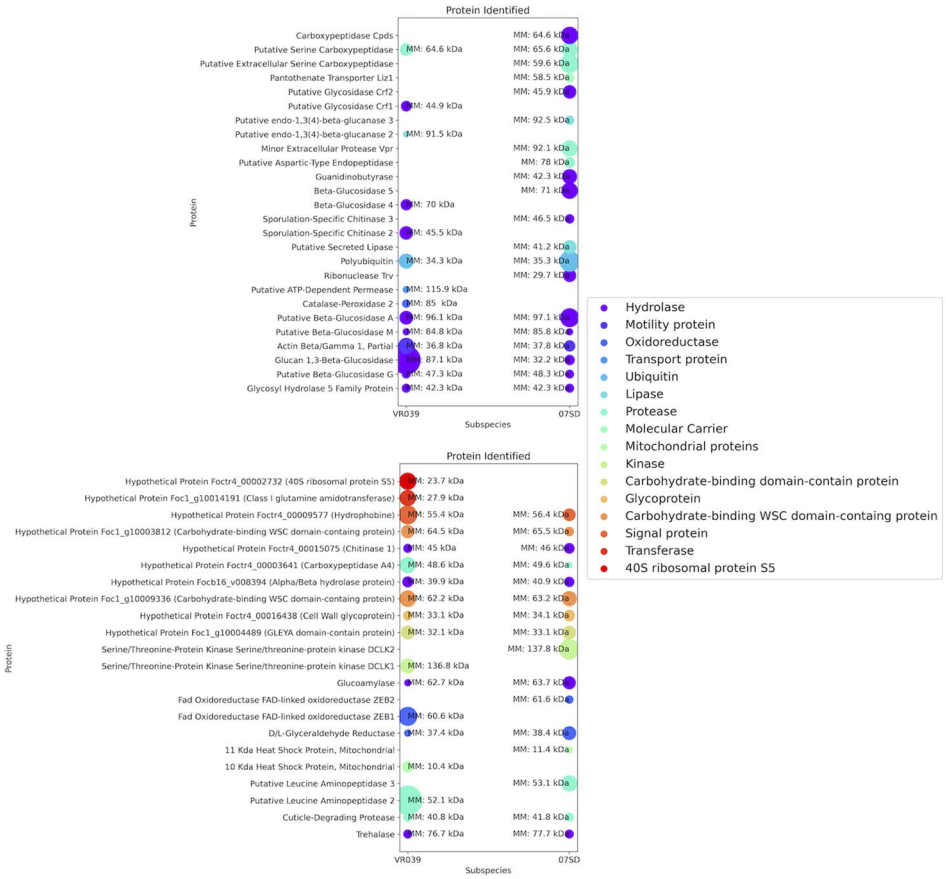

Fig. 6 Proteins identified within the silver nanoparticles of distinct *Fusarium oxysporum* strains (VR039 and 07SD). Each dot's size corresponds to the protein coverage detected during analysis. Colors represent specific protein classifications: purple (hydrolases), indigo (motility-associated proteins), blue (oxidoreductases), cyan (transport proteins), aquamarine (ubiquitins), light cyan (lipases), spring green (proteases), lime green (carrier proteins), yellow-green (mitochondrial proteins), yellow (kinases), gold (proteins with a carbohydrate-binding domain), red-orange (glycoproteins), red (signal proteins), deep red (transferases), and black red (40S ribosomal protein S5). Molecular masses (MM) of these proteins are indicated on each dot.

result may be associated not only with the similarities in size and morphology but also with the proteins present in the secretomes of the different strains of *Fusarium oxysporum*.

Within the proteins identified in the nanoparticles, the presence of ribonuclease stands out. Numerous studies have highlighted the effectiveness of RNase family in inhibiting the intracellular growth of various microorganisms, including *Mycobacterium*,[48,49] and even in the proliferation of biofilm structures of *Pseudomonas aeruginosa*.[50] Ribonuclease is an enzyme that plays a crucial role in nucleic acid metabolism, participating in RNA degradation. When incorporated into nanoparticles, ribonuclease assumes a remarkable antimicrobial function. Its mechanism of action involves the breakdown of RNA present in microorganisms, directly interfering with protein synthesis and genetic material replication.

The presence of FAD-oxidoreductase and other reductases in nanoparticles can play a significant role in promoting the formation of reactive oxygen species (ROS) within bacterial cells. These enzymes facilitate electron transfer processes that generate ROS as byproducts, which can accumulate to harmful levels. Elevated ROS levels induce oxidative stress, disrupting cellular functions, damaging essential biomolecules like DNA, proteins, and lipids, and ultimately leading to cellular dysfunction and death. This mechanism suggests that nanoparticles containing such enzymes might be effective in antibacterial applications by exploiting oxidative stress pathways to target and eliminate bacterial cells.[51–58]

The *Fusarium oxysporum* strains VR039 and 07SD exhibit distinct protein profiles; however, as shown in Fig. 7, these differences do not result in substantial variations in biological activity. In cases where a specific protein is absent in one strain, a homologous protein from the same family is often present, as seen with the putative glycosidases Crf1 and Crf2 in VR039 and 07SD, respectively. A similar pattern occurs with putative leucine aminopeptidase 2 and 3, which are exclusive to VR039 and 07SD, respectively. The primary differences in protein composition that could potentially influence biological activity include the minor extracellular protease Vpr, carboxypeptidase Cpds, putative extracellular serine carboxypeptidase, and putative aspartic-type endopeptidase. These proteins, which are involved in intracellular protein degradation, are present only in strain 07SD, suggesting a potential role in modulating strain-specific physiological responses.

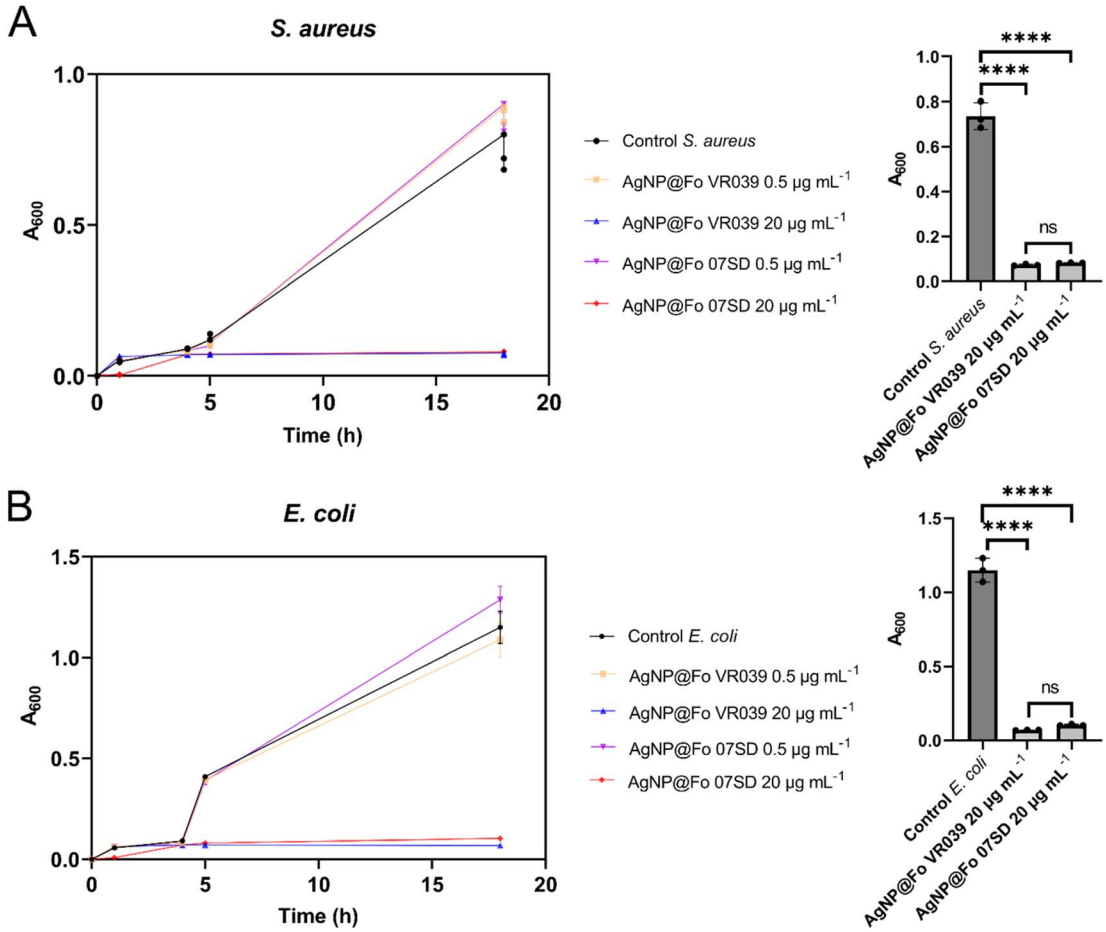

Fig. 7 Antimicrobial activity of silver nanoparticles (AgNP@Fo): (A) Evaluation of AgNP@Fo against *S. aureus* over different time points (h), measured by A_{600}, showing no significant difference in antimicrobial potential between AgNP@Fo VR039 and AgNP@Fo 07SD (ANOVA, $p < 0.0001$). (B) Test of AgNP@Fo against *E. coli* over different time points (h), also measured by A_{600}, revealing no significant difference in antimicrobial potential between AgNP@Fo VR039 and AgNP@Fo 07SD (ANOVA, $p < 0.0001$).

The evaluation of ROS production in *Staphylococcus aureus* treated with AgNP@Fo silver nanoparticles was conducted using concentrations of 0.6, 5.4, and 10.5 μg mL^{-1}. To detect ROS production, the fluorescent dyes acridine orange/ethidium bromide (AO/EB) were employed due to their capacity to differentiate viable from non-viable cells, as EB penetrates only cells with compromised membrane integrity, binding to nucleic acids and resulting in a red coloration. On the other hand, viable cells are permeable to AO, which stains DNA green.

After treatment with the nanoparticles, a significant decrease in green fluorescence intensity was observed as the concentration of AgNP@Fo VR039 increased. This indicates a reduction in cell viability dependent on the concentration, accompanied by an increase in red fluorescence, which suggests membrane damage and cell death (Fig. 8). These results suggest that AgNP@Fo can induce intracellular ROS production, promoting oxidative damage and leading to bacterial death. The oxidation of the AO/EB dye by ROS served as a marker for the generation of these reactive species within the intracellular environment, confirming the efficacy of the nanoparticles in promoting oxidative stress in *S. aureus*.

3. Conclusions

In conclusion, this study highlights the promising potential of AgNP biosynthesis using the biological system of *Fusarium oxysporum*, demonstrating an environmentally sustainable alternative compared to traditional chemical methods. Characterization of the synthesized nanoparticles revealed similar sizes between the AgNPs obtained using two fungal strains, and proteomic analysis identified proteins involved in the synthesis, stabilization, and antimicrobial activity of the AgNPs. The identification of redox proteins, such as glyceraldehyde reductase and FAD-oxidoreductase, suggests that the antimicrobial mechanism involves the generation of ROS, inducing oxidative stress in bacterial cells, as confirmed by bacterial growth inhibition assays and fluorescence microscopy. Additionally, these redox proteins are likely to be essential in the biosynthesis of nanoparticles, as their ability to reduce silver ions (Ag^{+}) to metallic silver (Ag^{0}) is fundamental to the formation of AgNPs. However, future research should explore the potential of other fungal strains with unique enzymatic profiles to enhance AgNP synthesis and stability. Additionally, optimizing culture conditions, such as pH,

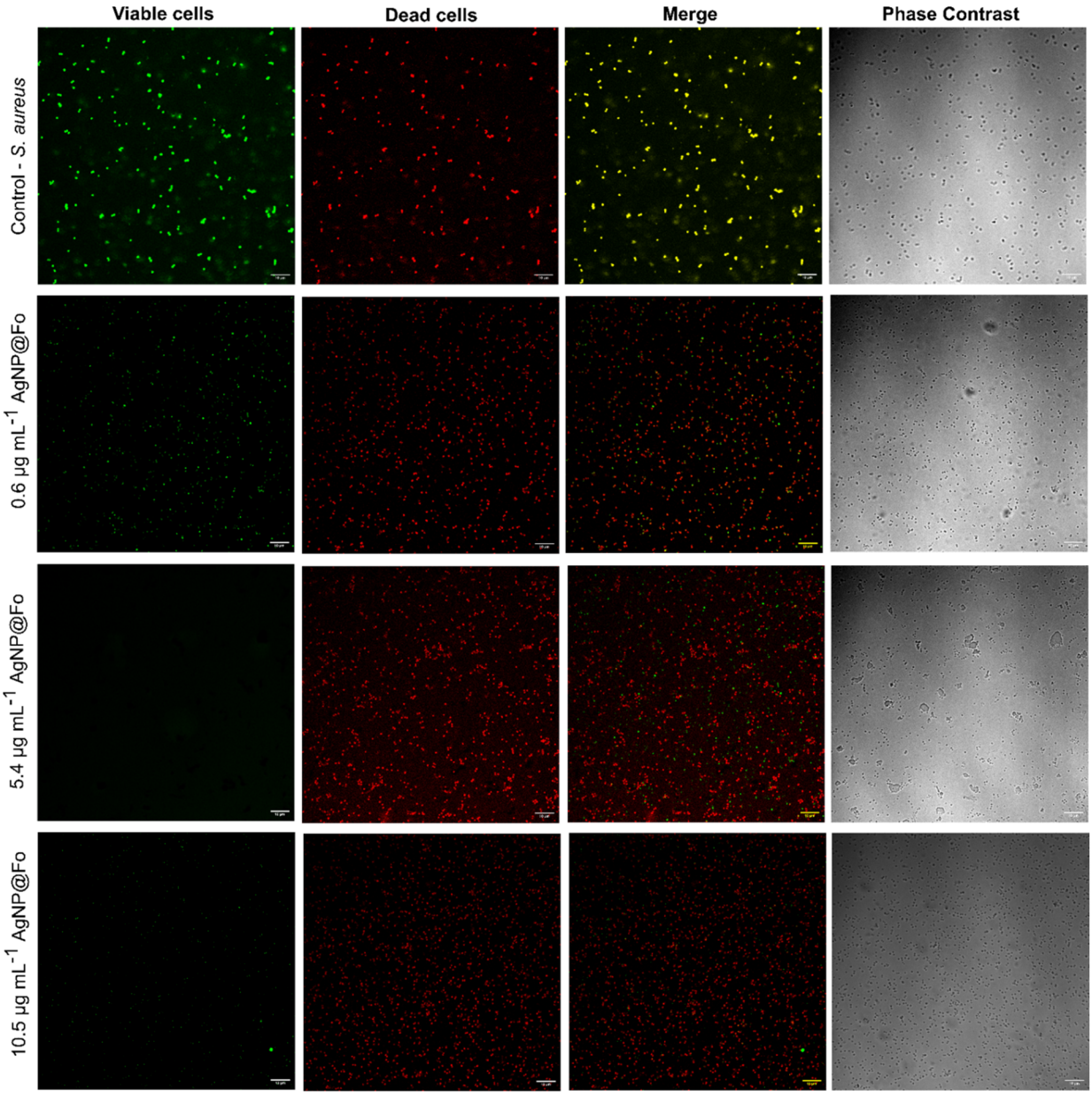

Fig. 8 Detection of ROS in *S. aureus* bacterial cells treated with different concentrations of AgNP@Fo (0.6, 5.4, and 10.5 µg mL^{-1}). Representative images from the live/dead cell viability assay in *S. aureus* were captured using fluorescence microscopy and phase contrast. Columns: 1 – viable cells; 2 – dead cells; 3 – merge; 4 – phase contrast. The white scale bar in the lower right corner of the images represents 10 µm.

temperature, and nutrient availability, could improve nanoparticle yield and properties.

Beyond demonstrating the efficacy of biosynthesized AgNPs, our findings underscore the potential of microbial secretomes as sustainable biocatalysts for nanoparticle production. By harnessing fungal systems for nanomaterial synthesis, this approach aligns with green chemistry principles, reducing the reliance on hazardous reagents and energy-intensive processes. The integration of such biogenic nanoparticles into biomedical, environmental, and industrial applications could pave the way for more sustainable nanotechnology solutions, promoting eco-friendly innovations in antimicrobial therapies and materials science.

4. Experimental section

4.1 Silver nanoparticle synthesis and testing of antimicrobial activity

Fungal biogenic silver nanoparticles (AgNP@Fo) were prepared according to the protocol described in the previous work of our research group[30] using the fungal filtrate prepared from the *Fusarium oxysporum* VR039 and *Fusarium oxysporum* 07SD biomass. The first step was to grow a culture of the fungus *Fusarium oxysporum* in Petri dishes using a culture medium of 0.5% yeast extract, 2% malt extract, and 2% agar. The inoculated medium was left for 7 days at 28 °C for fungus growth. After 7

days, a 500 mL liquid culture medium was made, consisting of 0.5% yeast extract and 2% malt extract. Approximately 1 cm^2 of the solid medium with the fungus was removed and transferred to the sterile liquid medium. The 500 mL culture medium was then incubated in a shaker under 150 rpm agitation at 28 °C for 6 days. The biomass obtained was filtered using filter paper and washed with deionized water. Approximately 10 g of biomass was weighed and put into 100 mL of deionized water. This material was stirred at 150 rpm at 28 °C for 3 days. The solution with biomass was then filtered using a Büchner funnel and filter paper (Qualy filter paper 9.0 cm diameter, 80 g^{-2} grammage, 205 mmol L^{-1} thickness, 14 mmol L^{-1} most pores), and the fungal filtrate (FF) was used for the synthesis of AgNP@Fo. Finally, $AgNO_3$ 1 mmol L^{-1} solution was added, and the reaction mixture was kept at 28 °C under protection from light.

Using dynamic light scattering (DLS) analysis, physicochemical properties such as hydrodynamic diameter, size distribution, polydispersity index, and surface charge were determined. The measurements were conducted using freshly prepared particle solution at 25 °C in a disposable DTS 1070 cuvette on a Zetasizer Nano-ZS ZEN3600 instrument (Malvern Instruments, Malvern, U.K.) equipped with a 4 mW He–Ne laser operating at 633 nm and a scattering angle of 173°. The data were collected in sets of 15 individual acquisitions, and the reported results represent the mean ± standard deviation (SD) based on three sequential measurements. The data were analyzed using Malvern Zetasizer software, version 7.11.

To observe the surface plasmon resonance (SPR) band of the nanoparticles, the UV-vis spectroscopy method with an Agilent HP 8453 spectrophotometer in the wavelength range of 200 to 1000 nm was employed. The size, and morphology of the nanomaterials were characterized using a Helios 5 PFIB CXe DualBeam transmission electron microscope.

The method for measuring bacterial growth at 600 nm (A_{600}) using a series of 96-well microplates with a multimode plate reader (EnSpire from PerkinElmer) was applied to evaluate the growth of *Staphylococcus aureus* and *Escherichia coli* in the Luria-Bertani broth (LB) medium. Each microplate contains 8 vertical rows (A to H) and 12 horizontal rows (1 to 12). The first column served as the positive control, containing 100 μL of bacterial inoculum combined with 100 μL of sterile LB medium. The second column was designated as the negative control, comprising 100 μL of sterile LB medium and 100 μL of AgNP@Fo colloids. The AgNP@Fo stock solution was diluted in sterile LB medium to maintain a final volume of 200 μL per well, followed by the addition of 50 μL of the inoculum suspension. Plates were incubated at 37 °C, and A_{600} readings were taken at various time points (0, 1, 2, 4, 5, and 18 h) to monitor bacterial growth and assess the antimicrobial activity of the AgNPs. Each experiment was conducted in triplicate for both *S. aureus* and *E. coli* to ensure reliability and facilitate comparisons of biological activity between the two microorganisms.

4.2 Detection of reaction oxygen species (ROS)

An acridine orange/ethidium bromide (AO/EB)-based dual-staining technique was applied to detect the release of ROS in both treated and untreated bacterial cells. The antibacterial effects of the nanoparticles (AgNP@Fo) on the studied organisms were assessed using a fluorescent microscope. Cell viability post-treatment was determined through the AO/EB staining method. A 50 μL aliquot of treated and untreated bacterial suspension was mixed with 50 μL of 10 μg mL^{-1} AO/EB solution and incubated for 5 min protected from light. After staining, a smear of the mixture was prepared on a glass slide and promptly examined under a confocal laser scanning microscope (Upright LSM780-NLO Zeiss microscope). In this procedure, alive cells stained with acridine orange exhibited green fluorescence, while dead cells stained with ethidium bromide fluoresced red.

4.3 Protein denaturation

Following the usual filtration steps for obtaining the fungal extract and silver nanoparticles, proteins were precipitated by successive additions of ammonium sulfate to 20 mL of the extract under magnetic stirring at 100 rpm and room temperature. At the first sign of turbidity and precipitate formation, the solution was kept for 16 h at 4 °C for complete precipitation. Subsequently, the mixture was centrifuged (5000 rpm, 10 min, 25 °C), and the supernatant was removed. The protein residue was then dissolved in 5 mL of sodium acetate buffer 10 mmol L^{-1}, pH 7.8, and dialyzed against the same buffer to remove excess salts, using a semipermeable membrane with a molecular weight cut-off of 3500 Da, changing the buffer every two hours twice and then, letting the salt exchange during 16 h at 4 °C. The resulting protein solution was then quantified using the Bradford method.

4.4 SDS gel electrophoresis

A 12% SDS-PAGE gel was prepared using secretome samples from two strains of *Fusarium oxysporum*, along with their respective nanoparticles (AgNP@Fo). Two staining methods were employed: silver staining and Coomassie blue staining. Silver staining was performed following the standard method outlined by J. M. Kavran[59] to detect low-concentration protein bands. For Coomassie blue staining, the gel was immersed in a 1% Coomassie blue R250 solution (containing 10% acetic acid and 50% ethanol) for 40 min. The gel was then destained in a solution of 10% acetic acid and 50% ethanol for 4 h. The electrophoresis was performed using PowerPac™ Basic Power from Bio-Rad.

4.5 In-gel digestion

Moving to the reduction step, 30 μL of 10 mmol L^{-1} 1,4-dithiothreitol (DTT) solution is added and incubated for 30 min at room temperature, then removed with a 30 s spin at 13 000 rpm. The next step is alkylation, where 30 μL of 50 mmol L^{-1} iodoacetamide (IAA) solution was added, and the mixture was incubated for 30 min at room temperature, protected from light. After a 30 s spin at 13 000 rpm, the IAA solution was removed and then, the gel was washed with 100 μL of 100 mmol L^{-1} ammonium bicarbonate for 10 min. Gel dehydration was performed with 200 μL of acetonitrile, incubating for 5 min at room temperature. For rehydration, the gel was exposed to 200

μL of 100 mmol L^{-1} ammonium bicarbonate for 10 min, removing the solution with a 30 s spin at 13 000 rpm and then, washed again with acetonitrile. For enzymatic digestion, a volume between 30 and 50 μL of the trypsin 20 ng μL^{-1} in ammonium bicarbonate solution was added, and the samples were rehydrated for 30 min on ice. The amount of trypsin added was adjusted based on the protein quantity in the band. After a quick spin to remove excess trypsin solution, 5 to 20 μL of 50 mmol L^{-1} ammonium bicarbonate was added to cover the gel and left overnight at 37 °C. The ammonium bicarbonate was removed with a 30 s spin at 13 000 rpm and then the extraction process was started by adding 10 μL of 5% formic acid in Mili-Q water or 30 μL for larger pieces. After 10 min, the gel was removed with a 30 s spin at 13 000 rpm, and the supernatant was treated with 12 μL of solution of 5% formic acid in 50% acetonitrile for 10 min. This step was repeated, and, then, the extracts were combined to evaporate the solvent, and the concentrated samples were stored at −20 °C for analysis.

4.6 Peptide desalting

The samples were then subjected to peptide isolation and purification using Oasis HLB solid-phase extraction (SPE) cartridges (Waters) with a 1 mL capacity and C_{18} phase. Initially, the cartridges were conditioned by eluting 1 mL of acetonitrile with 0.1% formic acid, followed by 1 mL of water with 0.1% formic acid. The samples were then loaded into the cartridge and desalted by eluting with 1 mL of water with 0.1% formic acid, and finally, the peptides were eluted by adding 1 mL of acetonitrile with 0.1% formic acid. The fractions from this last elution, which contained the peptides of interest, were subjected to vacuum drying in a SpeedVac concentrator (Thermo Scientific) until the solvent was eliminated.

4.7 Analysis by nanoflow nLC-MS/MS

An aliquot of peptides was analyzed on an ETD-enabled Orbitrap Velos mass spectrometer (Thermo Fisher Scientific, Waltham, MA, USA) connected to the EASY-nLC II system (Proxeon Biosystem, West Palm Beach, FL, USA) through a Proxeon nanoelectrospray ion source. Peptides were separated by a 2–90% acetonitrile gradient in 0.1% formic acid using an analytical column PicoFrit Column (20 cm × ID75 μm, 5 μm particle size, New Objective) at a flow rate of 300 nL min^{-1} over 65 min. The nanoelectrospray voltage was set to 2.2 kV and the source temperature was 275 °C. All instrument methods were set up in the data-dependent acquisition mode. The full scan MS spectra (m/z 300–1600) were acquired in the Orbitrap analyzer after accumulation to a target value of 1×10^6. The resolution in the Orbitrap was set to $r = 60\,000$ and the 20 most intense peptide ions with charge states ≥2 were sequentially isolated to a target value of 5000 and fragmented in the linear ion trap using low-energy CID (normalized collision energy of 35%). The signal threshold for triggering an MS/MS event was set to 1000 counts. Dynamic exclusion was enabled with an exclusion size list of 500, an exclusion duration of 60 s, and a repeat count of 1. An activation $q = 0.25$ and an activation time of 10 ms were used.

4.8 Proteomic data analysis

Raw data were processed using Sequest-HT as the search engine within the Proteome Discoverer informatics platform (version 1.4.0.288; Thermo Scientific), and MS/MS spectra were searched against *Fusarium oxysporum* f. sp. *cubense* from NBCI database. A tolerance of 10 ppm was considered for precursor ions and 1 Da for fragment ions, with a maximum of one missed cleavage. A fixed modification of carbamidomethylation of cysteine and variable modification of oxidation of methionine were considered. A 1% false discovery rate (FDR) was set for both the protein and peptide identification.

4.8.1 Hypothetical protein identification. The proteins labeled as hypothetical at *F. oxysporum* genome within the nanoparticle reaction media were subjected to investigation using the BLAST protein–protein online server, accessible on the NCBI website.[60] Default parameters were employed, and a minimum of four proteins with an identity percentage of 64% or greater were analyzed to categorize the hypothetical protein and delineate its function.

4.9 Statistical analysis

The experimental data are presented as mean ± standard deviation (SD). The size of the nanoparticles (nm) for each experiment is indicated in the corresponding figure legends. One-way analysis of variance (ANOVA) was employed to assess whether there were significant differences in antimicrobial potential among the different AgNP@Fo against *E. coli* and *S. aureus*. Differences were considered statistically significant with a p-value < 0.05, categorized as $*p < 0.05$, $**p < 0.01$, $***p < 0.001$, $****p < 0.0001$; and not significant (ns) for $p \geq 0.05$. All statistical analyses were conducted using GraphPad Prism (GraphPad Software, San Diego, CA, USA).

Data availability

Data for the article cannot be made available at the moment, due to legal confidentiality requirements, and a patent application (INPI, BR 10 2017 014836 0). All data will be publicly available as soon as the patent gets granted. If need further details, the corresponding author will provide data and information.

Conflicts of interest

There are no conflicts to declare.

Acknowledgements

The authors thank the funding by the Sao Paulo Research Foundation (FAPESP, Grants #2023/02338-0, and #2023/17118-6), and INCTBio (FAPESP, Grant #2014/50867-3), Coordination for the Improvement of Higher Education Personnel (CAPES, Finance code 001) and National Council for Scientific and Technological Development (CNPq, Grant #465389/2014-7). This research used facilities of the Brazilian Biosciences National Laboratory (LNBio) and the Brazilian National Nanotechnology Laboratory (LNNano) within the Brazilian Centre for

Research in Energy and Materials (CNPEM), a private non-profit organization under the supervision of the Brazilian Ministry for Science, Technology, and Innovations (MCTI). We kindly acknowledge the MAS staff for their assistance during the experiments (Proposal MAS-20221447)—likewise, the LNNano and Proposals TEM-C1 20233471, and TEM-FT 20230284.

References

1 A. Rozhin, S. Batasheva, M. Kruychkova, *et al.*, Biogenic silver nanoparticles: Synthesis and application as antibacterial and antifungal agents, *Micromachines*, 2021, **12**, 1480.
2 C. Joanna, L. Marcin, K. Ewa and P. Grażyna, A nonspecific synergistic effect of biogenic silver nanoparticles and biosurfactant towards environmental bacteria and fungi, *Ecotoxicology*, 2018, **27**, 352.
3 M. Malik, M. Iqbal, Y. Yqbal, M. Malik, S. Bakhsh, *et al.*, Biosynthesis of silver nanoparticles for biomedical applications: A mini review, *Inorg. Chem. Commun.*, 2022, **145**, 109980.
4 M. Malik, M. Iqbal, Y. Yqbal, M. Malik, M. Raza, *et al.*, Biosynthesis and Characterizations of Silver Nanoparticles from Annona squamosa Leaf and Fruit Extracts for Size-Dependent Biomedical Applications, *Nanomaterials*, 2022, **12**, 616.
5 N. Iram, M. Ahmed, N. Anwar, J. Ahmad, *et al.*, Chapter Three – Manufacturing nanoparticles using plants as nanofactories, *Compr. Anal. Chem.*, 2024, **107**, 49.
6 N. Anwar, M. Ahmed, N. Iram and P. Pham, Chapter Seven – Synthesis of nanoparticles and their applications in food processing, *Compr. Anal. Chem.*, 2024, **107**, 161.
7 N. Iram, S. Khan, M. Ahmed, A. Mir, N. Anwar, *et al.*, Synthesis and characterizations of silver nanoparticles-based conductive ink for high-frequency electronics, *Phys. Scr.*, 2024, **99**, 0859a8.
8 K. Gudikandula and S. Charya Maringanti, Synthesis of silver nanoparticles by chemical and biological methods and their antimicrobial properties, *J. Exp. Nanosci.*, 2016, **11**, 714.
9 V. Thiruvengadam and A. V. Bansod, Characterization of silver nanoparticles synthesized using chemical method and its antibacterial property, *Biointerface Res. Appl. Chem.*, 2020, **10**, 7257.
10 A. Ibrahim, Z. Ahmad, M. Z. Manzoor, *et al.*, Optimization for biogenic microbial synthesis of silver nanoparticles through response surface methodology, characterization, their antimicrobial, antioxidant, and catalytic potential, *Sci. Rep.*, 2021, **11**, 770.
11 E. Ibrahim, H. Fouad, M. Zhang, *et al.*, Biosynthesis of silver nanoparticles using endophytic bacteria and their role in inhibition of rice pathogenic bacteria and plant growth promotion, *RSC Adv.*, 2019, **9**, 29293.
12 T. Mustapha, N. Misni, N. R. Ithnin, *et al.*, A Review on Plants and Microorganisms Mediated Synthesis of Silver Nanoparticles, Role of Plants Metabolites and Applications, *Int. J. Environ. Res. Public Health*, 2022, **19**, 674.
13 M. Guilger-Casagrande and R. Lima, Synthesis of Silver Nanoparticles Mediated by Fungi: A Review, *Front. Bioeng. Biotechnol.*, 2019, **7**, 287.
14 K. S. Siddiqi and A. Husen, RAK Rao. A review on biosynthesis of silver nanoparticles and their biocidal properties, *J. Nanobiotechnol.*, 2018, **16**, 14.
15 H. Uzoeto, A. Nkiru, S. Aisida and F. Ezema, Enhanced microstructural properties and biocompatibility of Zinc oxide nanoparticles by biogenic synthesis protocol for antibacterial applications, *Hybrid Advances*, 2024, **7**, 100332.
16 H. Padinjarathil, M. Joseph, B. S. Unnikrishnan, G. U. Preethi, *et al.*, Galactomannan endowed biogenic silver nanoparticles exposed enhanced cancer cytotoxicity with excellent biocompatibility, *Int. J. Biol. Macromol.*, 2018, **118**, 1174.
17 S. Polash, Md. Hossain, T. Saha and S. Sarker, Biogenic Silver Nanoparticles: A Potent Therapeutic Agent. *Emerging Trends in Nanomedicine*, Springer, Singapore, 2021, p. 81.
18 X. Zhao, X. Xu, C. Ai, *et al.*, Advantages of silver nanoparticles synthesized by microorganisms in antibacterial activity, *Green Synthesis of Silver Nanomaterials*, 2022, p. 571.
19 D. Bamal, A. Singh, G. Chaudhary, *et al.*, Silver nanoparticles biosynthesis, characterization, antimicrobial activities, applications, cytotoxicity and safety issues: An updated review, *Nanomaterials*, 2021, **11**, 2086.
20 V. Novy, F. Nielsen, D. Cuellen, *et al.*, The characteristics of insoluble softwood substrates affect fungal morphology, secretome composition, and hydrolytic efficiency of enzymes produced by *Trichoderma reesei*, *Biotechnol. Biofuels*, 2021, **14**, 105.
21 Y. He, X. Zhou, J. Li, *et al.*, *In Vitro* Secretome Analysis Suggests Differential Pathogenic Mechanisms between *Fusarium oxysporum* f. sp. *cubense* Race 1 and Race 4, *Biomolecules*, 2021, **11**, 1353.
22 C. Zeiner, S. Purvine, E. Zink, *et al.*, Mechanisms of Manganese(II) Oxidation by Filamentous Ascomycete Fungi Vary With Species and Time as a Function of Secretome Composition, *Frontiers*, 2021, **12**, 610497.
23 E. Loshchinina, E. Vetchinkina and M. Kupryashina, Diversity of Biogenic Nanoparticles Obtained by the Fungi-Mediated Synthesis: A Review, *Biomimetics*, 2022, **8**, 1.
24 N. Durán, W. Fávaro, S. Alborés, T. Costa and L. Tasic, Biogenic Silver Nanoparticles Capped with Proteins: Timed Knowledge and Perspectives, *J. Braz. Chem. Soc.*, 2023, **34**, 897.
25 S. Raza, A. Ansari, N. Siddiqui, *et al.*, Biosynthesis of silver nanoparticles for the fabrication of non cytotoxic and antibacterial metallic polymer based nanocomposite system, *Sci. Rep.*, 2021, **11**, 10500.
26 W. R. Rolim, M. T. Pelegrino, B. L. Araújo, *et al.*, Green tea extract mediated biogenic synthesis of silver nanoparticles: Characterization, cytotoxicity evaluation and antibacterial activity, *Appl. Surf. Sci.*, 2019, **463**, 66.
27 V. Gopinath, S. Priyadarshini, M. F. Loke, *et al.*, Biogenic synthesis, characterization of antibacterial silver nanoparticles and its cell cytotoxicity, *Arabian J. Chem.*, 2019, **10**, 1107.

28 M. M. Hossain, S. A. Polash, M. Takikawa, *et al.*, Investigation of the Antibacterial Activity and in vivo Cytotoxicity of Biogenic Silver Nanoparticles as Potent Therapeutics, *Front. Bioeng. Biotechnol.*, 2019, **7**, 239.

29 F. Spagnoletti, F. Kronberg, C. Spedalieri, E. Munarriz and R. Giacometti, Protein corona on biogenic silver nanoparticles provides higher stability and protects cells from toxicity in comparison to chemical nanoparticles, *J. Environ. Manage.*, 2021, **297**, 113434.

30 T. Costa, M. Rodrigues, J. C. Jerônimo, *et al.*, Biogenic silver nanoparticles' antibacterial activity and cytotoxicity on human hepatocarcinoma cells (Huh-7), *RSC Adv.*, 2024, **14**, 2192.

31 R. Elamawi, R. Al-Harbi and A. Hendi, Biosynthesis and characterization of silver nanoparticles using *Trichoderma longibrachiatum* and their effect on phytopathogenic fungi, *Egypt. J. Biol. Pest Control*, 2018, **28**, 28.

32 S. R. K Pandian, S. Kunjiappan, V. Ravishankar and V. Sundarapandian, Synthesis of quercetin-functionalized silver nanoparticles by rapid one-pot approach, *Biotechnologia*, 2021, **102**, 75.

33 A. Almatroudi, Silver nanoparticles: Synthesis, characterisation and biomedical applications, *Open Life Sci.*, 2020, **15**, 819.

34 Carbohydrate-binding WSC, in: InterPro, **https://www.ebi.ac.uk/interpro/entry/InterPro/IPR002889/**, accessed Jan 2024.

35 S. Oide, Y. Tanaka, A. Watanabe and M. Inui, Carbohydrate-binding property of a cell wall integrity and stress response component (WSC) domain of an alcohol oxidase from the rice blast pathogen Pyricularia oryzae, *Enzyme Microb. Technol.*, 2019, **125**, 13.

36 M. Zámocký, Š. Janeček and C. Obinger, Fungal Hybrid B heme peroxidases – Unique fusions of a heme peroxidase domain with a carbohydrate-binding domain, *Sci. Rep.*, 2017, **7**, 9393.

37 A. Maddi, A. Dettman, C. Fu, *et al.*, WSC-1 and HAM-7 are MAK-1 MAP kinase pathway sensors required for cell wall integrity and hyphal fusion in Neurospora crassa, *PLoS One*, 2012, **7**, e42374.

38 J. T Mindrebo, C. M. Nartey, Y. Seto, *et al.*, Unveiling the functional diversity of the alpha/beta hydrolase superfamily in the plant kingdom, *Curr. Opin. Struct. Biol.*, 2016, **41**, 233.

39 M. Holmquist, Alpha Beta-Hydrolase Fold Enzymes Structures, Functions and Mechanisms, *Curr. Protein Pept. Sci.*, 2005, **1**, 209.

40 H. Heberle, G. Meirelles, R. F. Silva, P. G. Telles and R. Minghim, InteractiVenn: a web-based tool for the analysis of sets through Venn diagrams, *BMC Bioinf.*, 2015, **16**, 169.

41 L. Fricker and F. Rüth, Carboxypeptidase A4, *Handbook of Proteolytic Enzymes*, 2013, vol. 1, p. 1307.

42 M. Franceschetti, A. Maqbool, M. J. Jiménez-Dalmaroni, *et al.*, Effectors of Filamentous Plant Pathogens: Commonalities amid Diversity, *Microbiol. Mol. Biol. Rev.*, 2017, **81**, e00066.

43 M. Homthong, A. Kubera, M. Srihuttagum and V. Hongtrakul, Isolation and characterization of chitinase from soil fungi, Paecilomyces sp, *Agric. Nat. Resour.*, 2016, **50**, 232.

44 H. Merzendorfer, The cellular basis of chitin synthesis in fungi and insects: Common principles and differences, *Eur. J. Cell Biol.*, 2011, **90**, 759.

45 A. F. Ram, M. Arentshorst, R. A. Damveld, *et al.*, The cell wall stress response in Aspergillus niger involves increased expression of the glutamine: Fructose-6-phosphate amidotransferase-encoding gene (gfaA) and increased deposition of chitin in the cell wall, *Microbiology*, 2004, **150**, 3315.

46 M. Gholami-Shabani, A. Imani, M. Shams-Ghahfarokhi, *et al.*, Bioinspired synthesis, characterization and antifungal activity of enzyme-mediated gold nanoparticles using a fungal oxidoreductase, *J. Iran. Chem. Soc.*, 2016, **13**, 2059.

47 S. Xue, X. Zhang, X. Li, F. Zhao, *et al.*, Multi-pathways-mediated mechanisms of selenite reduction and elemental selenium nanoparticles biogenesis in the yeast-like fungus *Aureobasidium melanogenum* I15, *J. Hazard. Mater.*, 2024, **470**, 134204.

48 L. Bao, J. Hu, B. Zhan, *et al.*, Structural insights into RNase J that plays an essential role in Mycobacterium tuberculosis RNA metabolism, *Nat. Commun.*, 2023, **14**, 2280.

49 L. Lu, J. Arranz-Trullén, G. Prats-Ejarque, *et al.*, Human antimicrobial RNases inhibit intracellular bacterial growth and induce autophagy in mycobacteria-infected macrophages, *Front. Immunol.*, 2019, **10**, 1500.

50 D. Pulido, G. Prats-Ejarque, C. Villalba, *et al.*, A novel RNase 3/ECP peptide for Pseudomonas aeruginosa biofilm eradication that combines antimicrobial, lipopolysaccharide binding, and cell-agglutinating activities, *Antimicrob. Agents Chemother.*, 2016, **60**, 6313.

51 M. Y. Alkawareek, A. Bahlool, S. R. Abulateefeh and A. M. Alkilany, Synergistic antibacterial activity of silver nanoparticles and hydrogen peroxide, *PLoS One*, 2019, **14**, e0220575.

52 D. He, C. J. Miller and T. D. Waite, Fenton-like zero-valent silver nanoparticle-mediated hydroxyl radical production, *J. Catal.*, 2014, **317**, 198.

53 N. Thomas, D. D. Dionysiou and S. C. Pillai, Heterogeneous Fenton catalysts: A review of recent advances, *J. Hazard. Mater.*, 2021, **404**, 124082.

54 R. Canaparo, F. Foglietta, T. Limongi and L. Serpe, Biomedical applications of reactive oxygen species generation by metal nanoparticles, *Materials*, 2021, **14**, 53.

55 A. A. Dayem, M. K. Hossain, S. B. Lee, *et al.*, The role of reactive oxygen species (ROS) in the biological activities of metallic nanoparticles, *Int. J. Mol. Sci.*, 2017, **18**, 120.

56 N. Mammari, E. Lamouroux, A. Boudier and R. E. Duval, Current Knowledge on the Oxidative-Stress-Mediated Antimicrobial Properties of Metal-Based Nanoparticles, *Microorganisms*, 2022, **10**, 437.

57 F. Gao, T. Shao, Y. Yu, *et al.*, Surface-bound reactive oxygen species generating nanozymes for selective antibacterial action, *Nat. Commun.*, 2021, **12**, 745.
58 S. Chen, X. Yan, J. R. Peralta-Videa, *et al.*, Biological effects of AgNPs on crop plants: environmental implications and agricultural applications, *Environ. Sci.:Nano*, 2023, **10**, 62.
59 J. M. Kavran and D. J. Leahy, Silver staining of SDS-polyacrylamide gel, *Methods Enzymol.*, 2014, **541**, 16.
60 National Center for Biotechnology Information (NCBI), Bethesda (MD): National Library of Medicine (US), National Center for Biotechnology Information, **https://www.ncbi.nlm.nih.gov/**, accessed Jan 2024.